Plasmonic enhancement of thin-film solar cells using gold-black coatings

C.J. Fredricksen[a], D. R. Panjwani[b], J. P. Arnold[b], P. N. Figueiredo[b], F. K. Rezaie[b], J. Colwell[b], K. Baillie[b], S. J. Peppernick[c], A. G. Joly[c], K. M. Beck[c], W.P. Hess[c], R. E. Peale[b]

[a]LRC Engineering Inc., 9345 Chandon Drive, Orlando, FL, USA 32825;
[b]Dept. of Physics, University of Central Florida, 4000 Central Florida Blvd., Orlando, FL USA 32816;
[c]Environmental Molecular Sciences Laboratory at Pacific Northwest National Laboratory, Richland, WA USA 99352

ABSTRACT

Coatings of conducting gold-black nano-structures on commercial thin-film amorphous-silicon solar cells enhance the short-circuit current by 20% over a broad spectrum from 400 to 800 nm wavelength. The efficiency, i.e. the ratio of the maximum electrical output power to the incident solar power, is found to increase 7% for initial un-optimized coatings. Metal blacks are produced cheaply and quickly in a low-vacuum process requiring no lithographic patterning. The inherently broad particle-size distribution is responsible for the broad spectrum enhancement in comparison to what has been reported for mono-disperse lithographically deposited or self-assembled metal nano-particles. Photoemission electron microscopy reveals the spatial-spectral distribution of hot-spots for plasmon resonances, where scattering of normally-incident solar flux into the plane increases the effective optical path in the thin film to enhance light harvesting. Efficiency enhancement is correlated with percent coverage and particle size distribution, which are determined from histogram and wavelet analysis of scanning electron microscopy images. Electrodynamic simulations reveal how the gold-black particles scatter the radiation and locally enhance the field strength.

Keywords: plasmonics, thin-film, solar cell, metallic nanoparticles

INTRODUCTION

At present, the majority of the solar-cell market is based on crystalline silicon with thickness between 180-300 μm. This is much thicker than the characteristic absorption length for solar photons in silicon (several microns), so that material cost and weight are proportionally high. Thin film solar cells promise to reduce weight and costs. Thicknesses of 1-2 μm can be deposited on cheap substrates such as plastic. Thin film solar cells can be made with different materials such as α-Si, GaAs and CdTe, as well as organic semiconductors[1]. However, when the absorber material becomes very thin, it may become partially transparent and incapable of harvesting the entire solar flux. Therefore engineering solar cells to improve light trapping would improve efficiency.

This work investigates efficiency enhancement that occurs when small metal particles, in the form of gold-black, are deposited as scattering centers on the front surface of thin film solar cells. This increases the effective optical path length of incident light in the absorber layer and the fraction of the incident flux that is absorbed.

Increased effective path length within the absorber layers of such cells by deposition of small metal scattering centers is being pursued by many groups. Lithographically-produced or self-assembled arrays of metal dots have been shown to increase solar cell efficiency for at least part of the solar spectrum depending on geometry and size of deposited nano particles[2]. As an alternative approach, we investigated the possibility of using sparse depositions of gold black, a nano-structured metal formed by thermal evaporation in ~1 Torr inert ambient, giving a broad distribution of particle sizes[3-7]. The hypothesis is that the range of length scales inherent in such depositions will provide spectrally broad scattering to provide enhanced absorption across the entire solar spectrum.

The strong interaction of light and nanoparticles leads to creation of strong dipole radiation at the plasmon resonance frequency, resulting in an enhanced near-field intensity. The amount of light absorbed by the semiconductor is also increased, resulting in the generation of more electron-hole pairs. Dipole radiation generated from nano structures also increases the photon density in the nearby semiconductor. Plasmonic nanostructures are also capable of changing the optical properties near the semiconductor surface, which can increase the absorption of light[8], in principle.

This mechanism provides an excellent opportunity to reduce the physical thickness of the absorber while maintaining sufficient optical thickness. A thinner absorber has less bulk recombination and gives higher open circuit voltage, V_{oc}, across the junction for the same photo-generated charge. Scattering provides an elongated optical path length for photons that enter the absorber layer at oblique angles and may allow them to become trapped inside the semiconductor by total internal reflection. This longer path length exponentially increases the amount of light absorbed, resulting in higher production of electron hole pairs, and thus higher short circuit current, I_{sc}. For these reasons, it is possible to enhance the efficiency of thin film solar cells using plasmonic nano structures at the front surface. Moreover, metal nano particles as scattering centers can be applied to any thin absorber, not just silicon[9].

Many groups have shown that lithographically produced or self-assembled arrays of metal nano particles increase efficiency of thin film solar cells[2]. The absorption and scattering of nano particles is size and wavelength dependent, so it is important to optimize the particle size to ensure the maximum scattering occurs in the spectrum of interest. Absorption dominates when the particle size is < 50 nm, leading to localized heating. This can be very useful for thermal detectors but in the case of solar cell applications we need the maximum amount of scattering. Scattering occurs when particle size is more than 100 nm, however particle size should not be too large, as it would lead to multipole oscillations, which would eventually reduce the scattering[10].

Though it is possible to control the size and pitch of the nano particles specifically using lithography, the disadvantage of following this route is that the photocurrent enhancement is achieved in only a specific range of the solar spectrum depending on size and geometry of the deposited particle. Moreover, the production of metal nano particles through photolithography is expensive.

Gold black is produced cheaply and quickly in a low-vacuum process using the method of Harris, requiring no lithographic patterning[3-7]. Gold black has broad size distribution depending on deposition parameters such as inert gas pressure, deposition rate and the initial mass of the gold[11-15]. The density of gold black is much less than that of bulk gold. The packing fraction and particle size can be easily controlled by inert gas pressure[16]. Thus, these coatings have the potential to enhance light-harvesting efficiency over a broader range of the solar spectrum than lithographically patterned metals. For thermal detectors, thick opaque films are required[17]. For solar cells, a thin film is needed to allow scattered light to reach the semiconductor without shading the surface.

METHODOLOGY

Very thin, porous films of gold black with low packing fraction were first deposited on a substrate by thermal evaporation in a chamber that was back-filled to ~1 Torr with N_2. At such pressures, the evaporated metal particles are able to combine into nano-scale agglomerates before reaching the substrate. For the current work, each evaporation used ~1 mg of gold in a Molybdenum boat and proceeded until all the gold in the boat was exhausted.

For this work, each deposition covered two separate substrates simultaneously. Along with the solar cell, a 1 cm^2 square double-side-polished silicon substrate was coated for convenient characterization of the film by SEM and PEEM (Photo Emission Electron Microscopy). Both the silicon substrate and the solar cell were mounted on copper holders to dissipate heat absorbed during the thermal evaporation process.

Steps to deposit gold black film are as follow. The chamber is evacuated to a pressure of $<10^{-4}$ Torr with a roughing pump, followed by a diffusion pump. The substrate is cooled to ~30 ^{0}F. Current of 50-70 A is passed through the Mo boat to evaporate the gold contained within. The current is turned off, and the temperature of the substrate brought up to room temperature to avoid condensation when the chamber is vented.

We performed the deposition of gold black on two different types of solar cells. The first type was a standard thick single crystal solar cell and the second was a commercial amorphous thin film solar cell (PowerFilm). Two level full factorial experiments[18] were performed on thick crystal Si cells first as a control. No improvement was expected for such thick cells, since they absorb all the light anyway, and experiments confirmed this. These experiments established our deposition, characterization, and statistical analysis procedures. Second, we investigated thin-film α-Si solar cells. Here an efficiency enhancement effect was expected to be possible and was confirmed.

The statistical approach to the experiment is presented in Table 1. The independent variables (x1, x2, x3) are the pressure of the buffer gas, the current through the boat (which determines the evaporation rate), and the starting mass of gold. Upper limit values of the independent variable are denoted by "+" and lower limit values are denoted by "-". A 2 level full factorial experiment requires two sets of eight runs (2^3), one for each combination of the three parameters. Additionally, four runs are performed at the mid points of the parameter ranges for a confidence level of 95%. The middle points are denoted by "*" in the table. The dependent variables, or responses, are the change in efficiency and the percent surface coverage. The order of the film preparation was randomized to avoid systematic effects. Interactions between the dependent variables have been analyzed and response surfaces plotted in order to find the maxima.

Run	x1	x2	x3
1	-	-	+
2	-	+	+
3	+	-	+
4	+	+	+
5	-	-	-
6	+	-	-
7	+	+	-
8	-	+	-
9	*	*	*
10	*	*	*
11	+	+	-
12	+	+	+
13	+	-	-
14	-	-	-
15	-	+	+
16	-	+	-
17	+	-	+
18	-	-	+
19	*	*	*
20	*	*	*

Table 1 Two-level full factorial protocol and order of experiments

From the data collected for samples according to parameter values in Table I, we may predict responses at other parameter values according to Eq. 1

$$Y_{PR} = a_0 + a_1x_1 + a_2x_2 + a_3x_3 + a_{12}x_1x_2 + a_{13}x_1x_3 + a_{23}x_2x_3 + a_{123}x_1x_2x_3 \,, \qquad (1)$$

where the coefficients a_n are determined from the factor effects and x_n are the factor variables[18].

DATA AND RESULTS

1.1 Measurements

We measured the net conversion efficiency of standard Si solar cells with & without gold-black deposited on the surface. Figure 1 presents photos of the evaporator, optical measurement setup, and electrical test circuit for measuring the IV characteristics. Figure 1 (left) shows the copper bar electrodes with Moly boat clamped between them and the sample stage adjacent to the boat. The sample is cooled using a Peltier cooler sandwiched between a copper heat sink with water cooling on the warm side and a copper cold plate on the cold side. The sample is mounted on the copper cold plate, along with the silicon substrate for convenient analysis by SEM, etc. Figure 1 (center) shows the optical test

setup. The Xe arc lamp marked A in the photo is positioned at the entrance port of the monochromator. Light exits the monochromator towards the top of the photo, where the collection optics marked C direct it onto the sample at position D. For broadband measurements of overall efficiency, the Xe lamp is moved to position B and a filter set (AM0 and AM1.5) is positioned in front of the lamp. The photo current (I_{sc}) response is recorded for solar cells with different gold-black depositions across the wavelength range of 350 to 1100 nm using the monochromator. The data was collected and displayed in Labview.

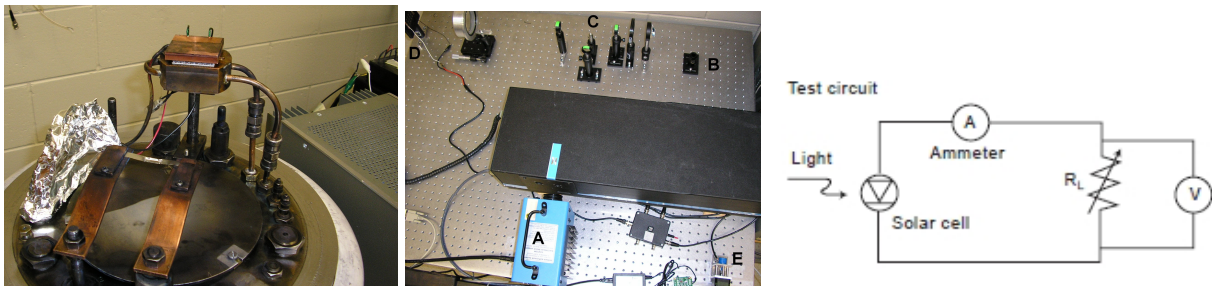

Figure 1 (left) – Photo of the thermal evaporation system. Figure 1 (center) – The Xenon arc lamp is moved between positions A (monochromated light) and B (broadband solar spectrum). A plane mirror is inserted at position C for monochromated light and removed for broadband solar spectrum illumination. The DUT is located at position D and the stepper-driven potentiometer is at E. Figure 1 (right) – Schematic of test circuit.

The electrical characterization of solar cells under broadband illumination, shown schematically in Fig. 1 (right), results in an IV curve as shown in Figure 2. Load resistance is varied under computer control using a stepper-driven potentiometer (labeled "E" in Fig. 1, center). Subsequent measurements on thin film solar cells benefited from an upgrade of the system due to the acquisition of a Keithley SourceMeter, shown in Fig. 3.

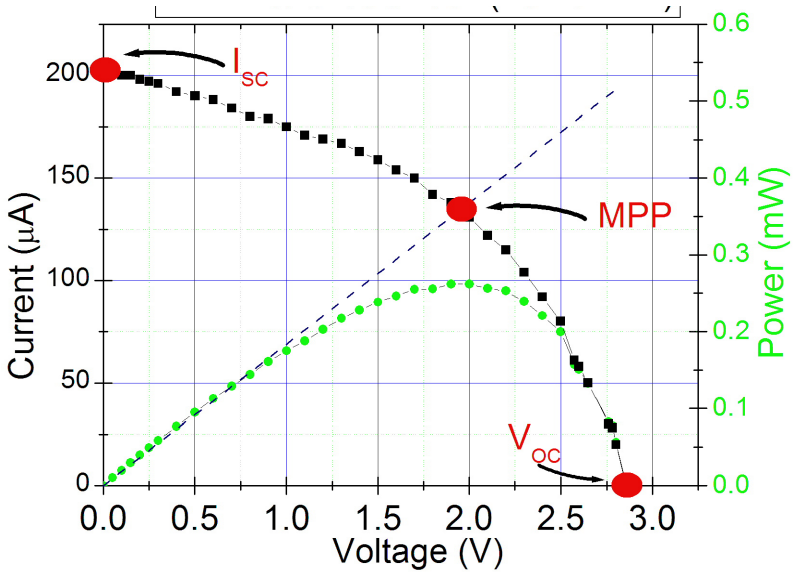

Figure 2 - IV curve, measured with the configuration in Fig. 1, plotted along with power vs. voltage (circles). MPP (maximum power point) occurs at the knee.

The intersection with the voltage axis at zero current gives the open circuit voltage (V_{OC}). The intersection with the current axis at zero applied voltage gives the short circuit current (I_{SC}). The optimum operating point is at the "knee" of the curve, where the power has its maximum value. The Maximum Power Point (MPP), I_{SC}, and V_{OC} are indicated on the plot. The slope of the dashed line identifies the optimum load resistance. The solar cell efficiency is determined by

$I_m V_m$/(incident optical power). Photocurrent enhancement factor is defined in terms of short circuit current by $E = I_{sc}^{(p)}/I_{sc}^{(ref)}$, where the numerator corresponds to the measurement with particles on the surface.

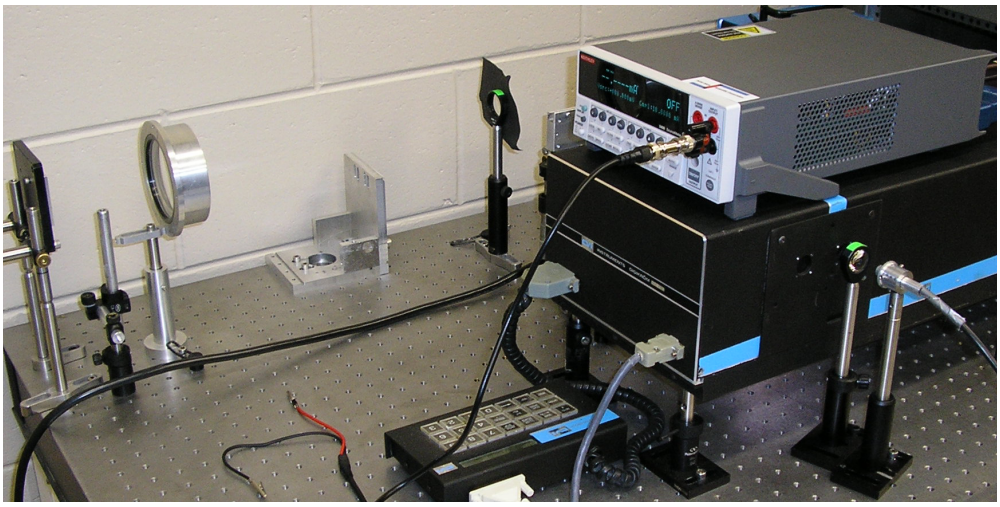

Figure 3 - Photograph of upgraded solar cell characterization facility with Keithley SourceMeter.

1.2 Percentage coverage & Wavelet Analysis

SEM images determined the relationship between the controlled parameters and the morphology of the nanoparticles. Example images are presented in Figs. 4 and 5. The percent coverage was found from histograms of such images, i.e. from the ratio of the number of bright pixels (gold-black) to the total number of pixels in the image (Figures 4 and 5, right). The dark peak of the histogram corresponds to the substrate, while the bright shoulder is due to the gold-black. To separate them for the area analysis, the dark peak was assumed to be symmetrical.

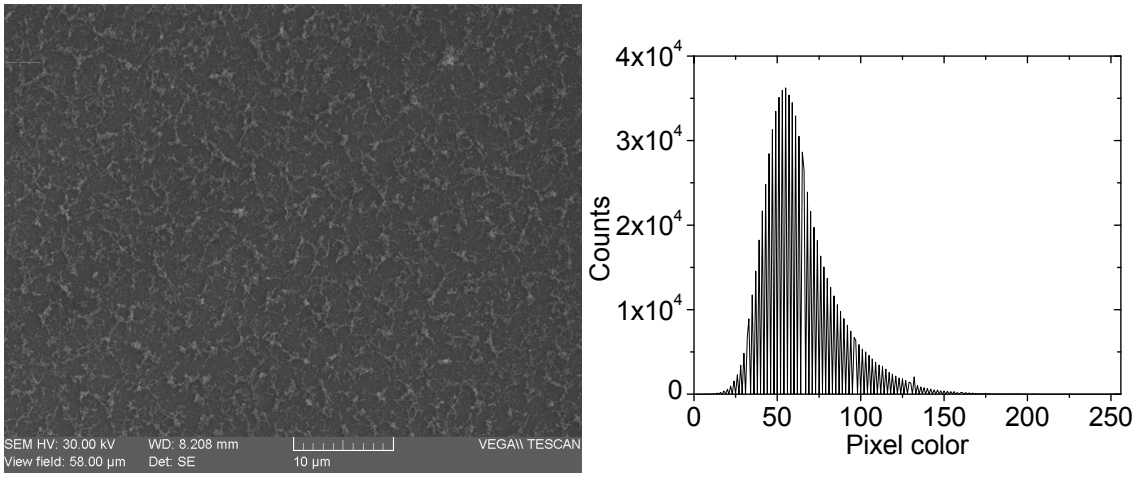

Figure 4 - (left) SEM image of lightly coated substrate. Gold black film run #18 (0.5 mg Au, 400 mTorr, 68A). (right) Histogram generated from this image. The fraction of coverage by gold-black was determined from the tail of the histogram that extends beyond ~100 on the brightness scale.

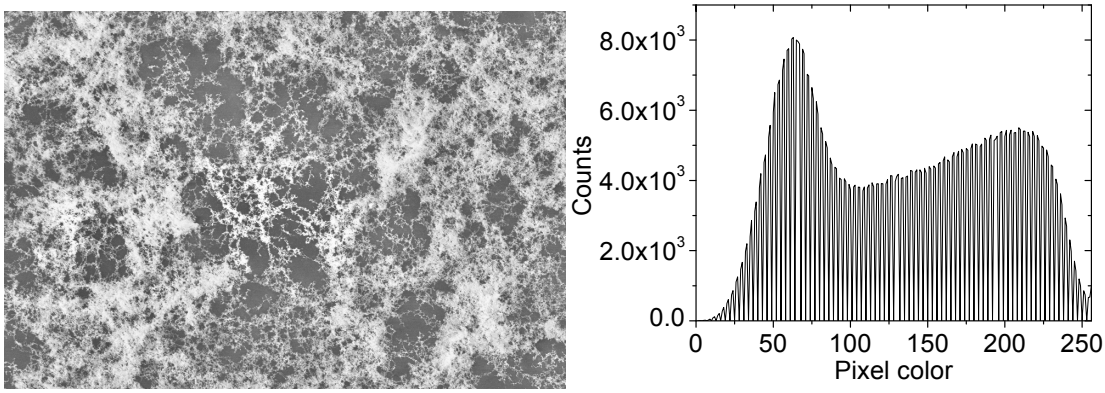

Figure 5 - SEM image and histogram of heavily coated sample. Sample 6x (run #12 – 1.5 mg Au, 1000 mTorr, 68 A).

Wavelet analysis for the image in Fig. 4 is plotted in Fig. 6. The peak shows that the mean feature size occurs at ~2.3 μm. The distribution of feature sizes ranges from < 100 nm to 20 microns. It is important to note that the wavelet analysis was performed on SEM images with large fields of view. Thus, the peak obtained is more indicative of the disperse nature of the open network rather than of the size of the particles. Performing this analysis on higher quality images over smaller fields of view will focus the results on the size of the particles rather than on feature size.

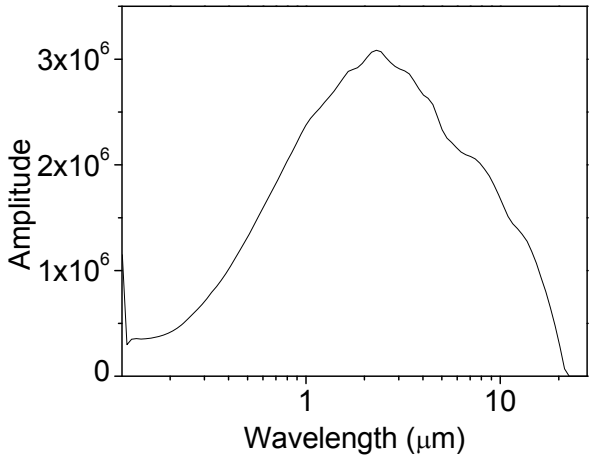

Figure 6 - Results of wavelet analysis for the image in Fig. 4.

This broad distribution of particle sizes may be responsible for the broad spectral range of the resonant enhancement for the entire spectrum in case of thin film solar cell as result shown in section 3.4. Once data of percentage coverage and wavelet analysis is collected for full factorial deposition parameters, one can be in better position to conclude what average particle size is sufficient to ensure maximum scattering and avoid absorption.

1.3 Full factorial results

The full factorial analysis was performed for thick crystalline silicon solar cells. Figure 7 shows response surfaces for efficiency, taken at the middle points at constant current (left) and constant pressure (right). The maximum appears at the lowest mass of gold and the lowest evaporation boat current (or lowest evaporation rate). The net change in efficiency was negative for all of these thick crystalline silicon samples, as anticipated. The response surface confirms our interpretation, namely that small metal particles simply shade optically thick cells, so that less coverage is better.

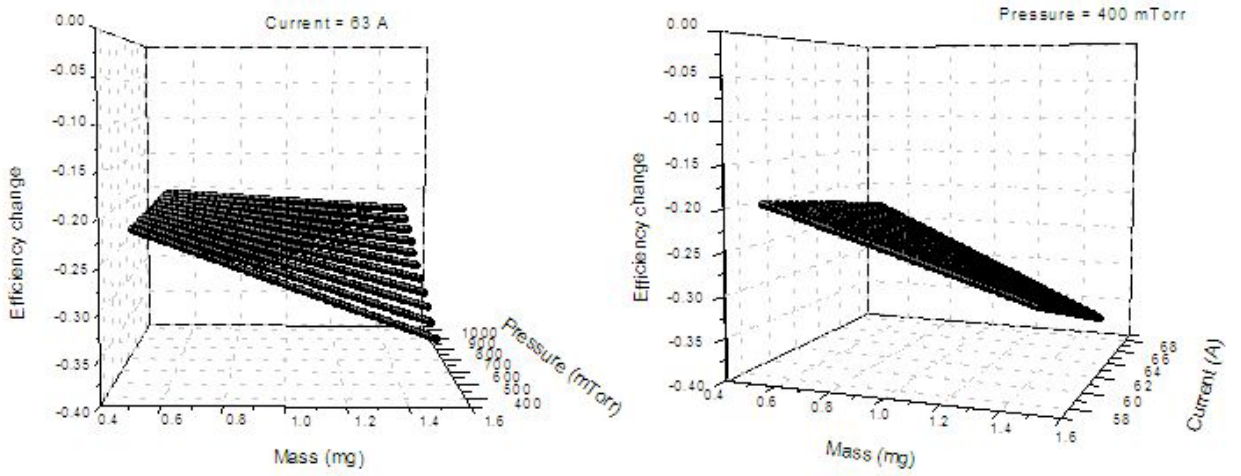

Figure 7 - Response surfaces for efficiency, plotted as a function of gold mass and pressure at constant boat current (left) and as a function of gold mass and evaporation boat current at constant pressure (right).

Response surfaces for coverage are plotted in Figures 8 and 9. The minimum at lowest current and lowest mass in Figure 8 shows that smaller masses (obviously) and lower evaporation rates will lead to lower percent coverage.

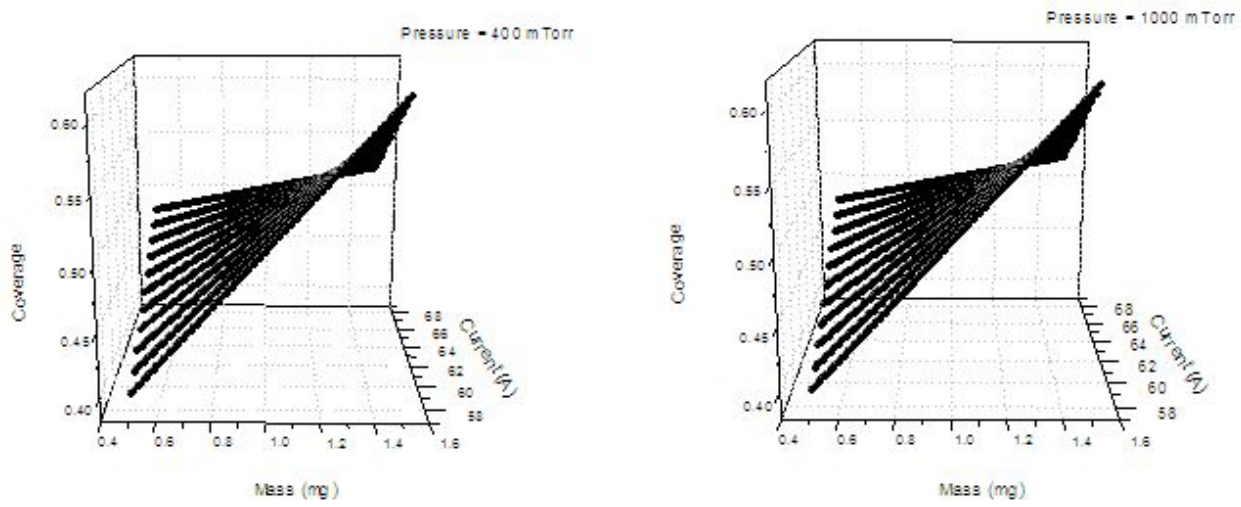

Figure 8 - Response surfaces for percent coverage at constant pressure.

The response surfaces in Figure 9 show results that are not intuitively obvious. Minima at lowest pressure and *higher* mass provide some insight about the effect of pressure on the morphology. At lower pressures, the goldblack layer is a more open network; at higher pressures the density is higher. The maximum in the change in efficiency at higher pressures (Figure 7, left) seems to imply that the more dense morphology may be more effective, albeit at thinner layers to avoid shadowing.

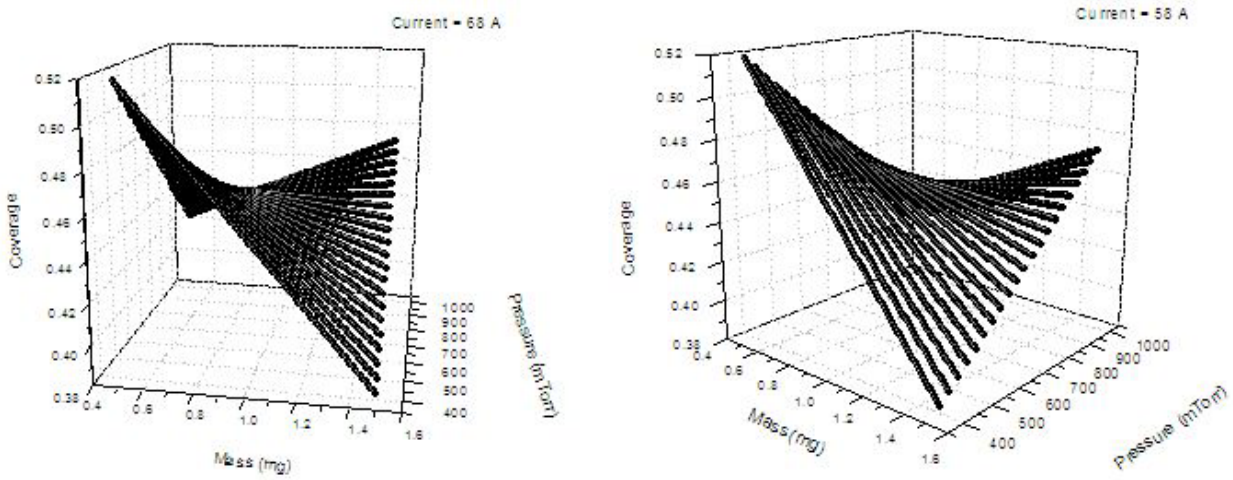

Figure 9 - Response surfaces for percent coverage at constant current.

1.4 Thin film solar cell results

The thin film solar cell investigated was an amorphous silicon cell from Power Film. This is sufficiently thin that it is flexible. The absorption coefficient of amorphous silicon decreases sharply in infrared, but there is still significant photocurrent generated out to wavelengths of 1100 nm as shown in Fig. 10.

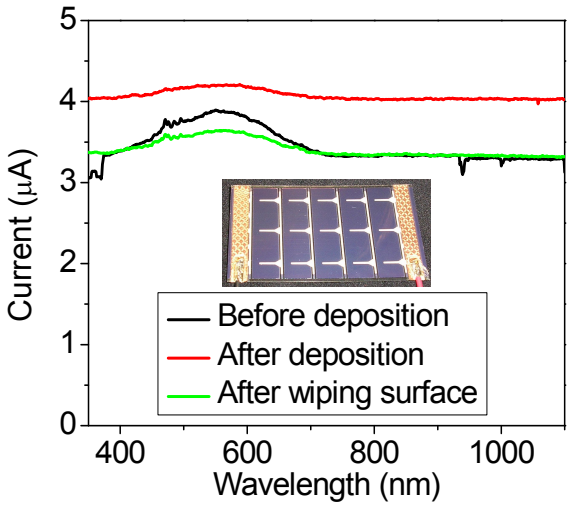

Figure 10 - Demonstration of photocurrent increase across the spectrum for thin film solar cell coated with gold-black particles. Photocurrent was measured under zero applied voltage. The inset is a photo of the sample under test.

After deposition of gold-black on the surface, the photocurrent increased by ~20% at most wavelengths, while the improvement was less (~10%) at the peak of the photo response at 580 nm, namely the improvement in photo response caused by scattering centers on the surface should be strongest at those wavelengths where the absorption by the film alone is weakest. The improvement disappeared when the deposited metal particles were wiped off. Unfortunately, the gold-black coating was removed from this sample before I-V measurement was performed. Another sample showed 6.9% efficiency increase and 12% improvement in I_{sc} photocurrent response (Fig. 11).

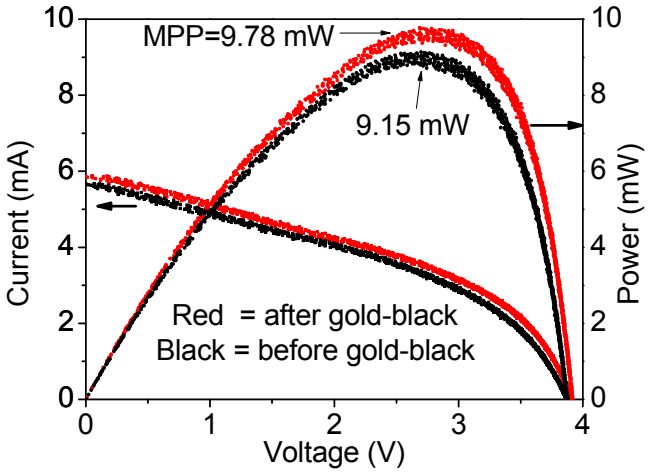

Figure 11 - IV and photo-power curves for PowerFilm amorphous silicon solar cell for solar spectrum irradiance. Also indicated on the IV curve is the Maximum Power Point (MPP). The maximum power point before deposition was 9.15 mW. After deposition, the maximum power point increased by 7%.

These results confirm that deposition of gold black with the 'right morphology' increases the efficiency of thin film solar cells. It remains to identify the deposition conditions that optimize the increase and to correlate the increase with film characteristics in order to obtain an understanding based on physics. The former goal remains for future work. Some progress toward the latter goal is described next.

1.5 Photoemission Electron Microscopy (PEEM)

This technique provided information about the spatial distribution of the plasmon resonances, which can be correlated with SEM images and IV measurements. PEEM uses a near infrared laser to excite Plasmon resonances, and it gives a visual indication of field enhancement by detecting electrons emitted from the thin films that are within the field of view of the instrument. PEEM uses a cooled CCD camera to record photoelectron emission from samples that are irradiated using sources such as mercury arc lamps and lasers. Wavelength tuning in the visible and near infrared causes resonances to appear in different parts of the sample surface due to the distribution of particle sizes and surrounding dielectric environments.

Fig 12 (right) presents PEEM images from gold-black samples using Hg lamp excitation. The emission that occurs is enhanced at the plasmon resonances. The lower left quadrant has been modified by a focused ion-beam mill (FIB) to make a marker for alignment. First, we notice that the modified surface has different morphology in the SEM image and is less bright in the PEEM image, showing that it has less plasmon activity. Second, the distribution of bright-white hotspots in the PEEM image is less dense in the modified region than one might expect from the distribution of comparable structures in the SEM image. These results suggest that there is a range of parameters that effect plasmon activity, giving wide scope for optimization.

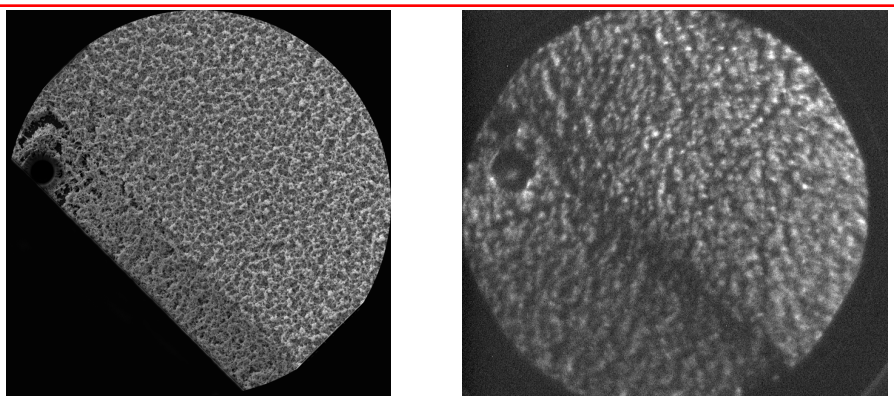

Figure 12 - SEM image (left) of a gold black sample. PEEM image of the same sample under Hg lamp illumination (right). The field of view is 150 microns.

Fig. 13 presents preliminary results of the wavelength dependence for the PEEM images. The two wavelengths are not very different, and consequently, the hot-spot distribution for the two images is nearly identical. Nevertheless, the image for the longer wavelength shows more contrast, i.e. the hot spots are brighter relative to the background. We suggest that this is because the wavelength is now closer to the surface plasmon resonance wavelength for gold (~500 nm).

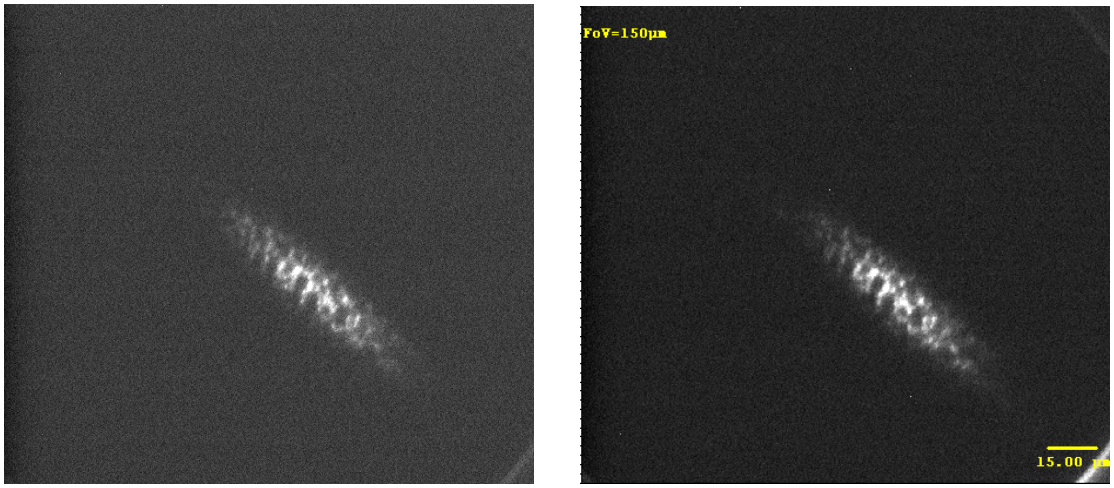

Figure 13 - Gold black sample illuminated by a laser at two different wavelengths. (left) λ = 370 nm and (right) λ = 420 nm.

PEEM images of gold-black films with 50 micron field-of-view are presented in Fig. 14. The bright areas correspond to photoelectron emission for laser illumination at 370 nm (left) and 420 nm (right) wavelengths. Again we see higher plasmon activity in the longer wavelength image when we are closer to the bulk surface plasmon resonance wavelength of gold.

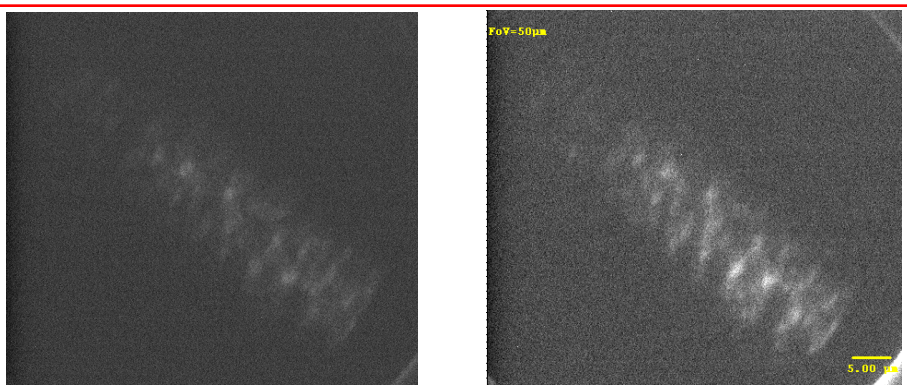

Figure 14 - Left: PEEM image of gold black film under λ = 370 nm laser illumination. Right: under λ = 420 nm laser illumination.

"Hot spots" at each of the wavelengths are relevant to photovoltaic power generation. It is in principle possible to optimize the parameters of deposition providing highest density of "hot spots" when irradiated with source in the range of 400-800 nm.

1.6 Simulation

Electrodynamic simulations and physical characterization can inform future optimization to obtain higher efficiency enhancements. For the experimental characterization, we have employed Scanning Electron Microscopy (SEM) and Photoemission Electron Microscopy (PEEM). The SEM images may be analyzed to obtain percent coverage and particle size distributions. PEEM images can give spectral and spatial distributions of plasma resonance hot spots, where optical scattering is enhanced. Electrodynamic simulations can reveal scattering and field enhancements, where film parameters can be quickly changed and optimized using a computer.

Through simulation one can visualize any system of nano particles on a substrate, to see how the intensity of an incident field is behaving at different cross sections of the system, such as inside the substrate or close to the nano particle. We generated a system with nano-scale gold spheres placed on the surface of an optically thin silicon layer. The software package Lumerical solved Maxwell's equations over a variable meshed field, giving spatial and spectral profiles of intensity enhancements. The 3 dimensional layout is presented in Figure 15. This model has 100 nm diameter gold spheres located 100 nm from the surface of a 200 nm thick silicon wafer. The 532 nm light source is incident from underneath and confined to the region defined by the white borders.

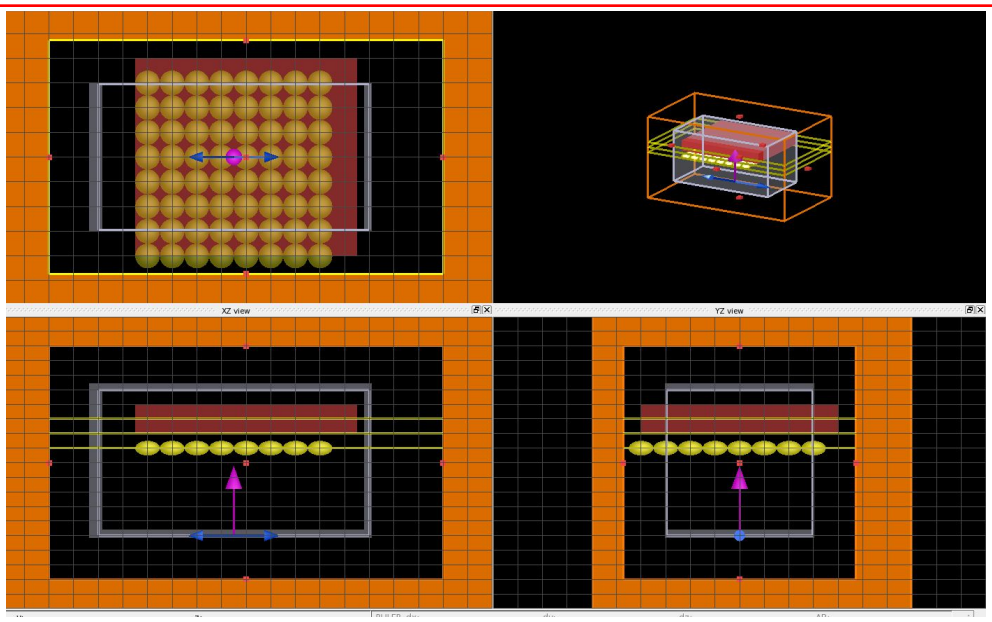

Figure 15 - The model system for electrodynamic simulation using Lumerical. A layer of 100 nm gold spheres is located 100 nm in front of the surface of a 200 nm thick silicon wafer. Radiation is incident from outside the wafer (purple arrow). Blue arrows indicate the polarization and the grey boxes define volume in which the radiation is confined.

Fig 16 presents results of the simulation according to a monitor placed on the surface of the silicon. Bright colors (top of the color scale and red in the color image) show field enhancement. The presence of bright red color at the top and bottom edge of the silicon slab are evidence of lateral scattering by the metal particles and waveguiding by the slab to its ends, where the light emitted. This light is much more intense (by an order of magnitude) than the incident intensity, as evidenced by the light that passes around the edges of the silicon at left and right. The smaller bright red patches at the right and left edges of the silicon slab show that the direction of the scattering depends strongly on the polarization of the incident polarized beam.

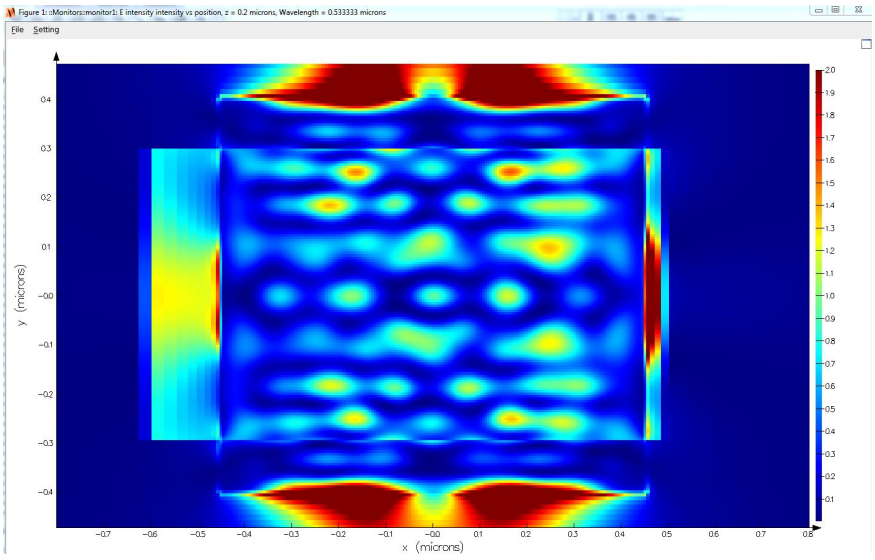

Figure 16 - A monitor at the surface of the silicon wafer, showing the spatial profile of the intensity of the radiation. The highest intensity is the top of the color scale (red in color image).

Fig. 17 presents the intensity pattern according to a monitor placed in the plane of the metal particles. The field is zero within the metal particles as expected, but it is strongly enhanced by an order of magnitude on the surfaces of the spheres. The enhancement is stronger to the right and left, indicating the polarization dependence.

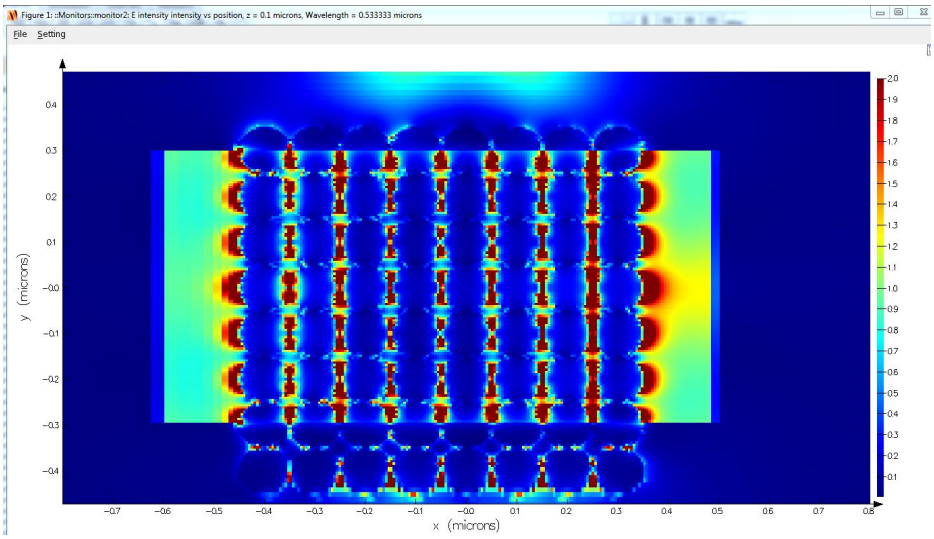

Figure 17 - A monitor in the plane through the center of the layer of gold particles. High intensity is seen around the edges of the gold spheres and none is seen inside the metal, as expected.

Fig. 18 presents the intensity according to a monitor within the thin silicon slab. This section is the most important of the three, since we need scattering inside the active layer. The field is strongly enhanced within the slab by an order of magnitude as a consequence of resonant scattering by the metal particles. Moreover, the high intensity bleeding out the ends of the slab at top and bottom shows that the scattered radiation is being channeled like a waveguide by the silicon, giving a substantial increase in the effective optical path length.

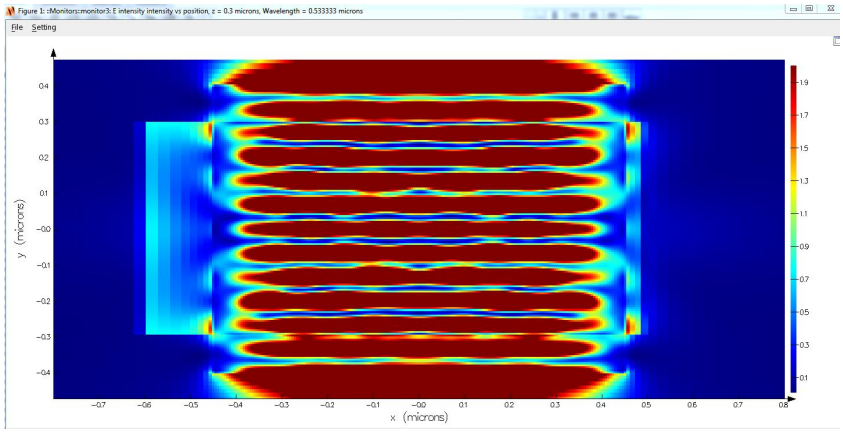

Figure 18 - A monitor 100 nm inside the silicon surface. The bright red regions show the very high intensity enhancement due to the gold nanoparticles.

The enhancement depends on the wavelength of incident radiation and on particle size. Once we find parameters producing desirable gold black morphology we can visualize the intensity enhancement and compare it with PEEM analysis of the same sample. Simulations can provide an understanding of the behavior of the enhanced field, so it is possible to make experimental changes in deposition parameters for even better results.

CONCLUSION

We initiated our experiment of depositing gold black as scattering centers for standard thick crystal Si solar cells as a control. Though none of the results in full factorial experiment show efficiency improvement for these thick cells, it helped us to optimize the deposition, characterization, and analysis procedures, which eventually proved useful in our successful demonstration of efficiency enhancement for a thin film solar cell.

The initial experiments on thin film solar cells showed 20% increase in short circuit photocurrent response across a major part of the spectrum, while 10% photocurrent enhancement was seen in the visible band where the solar cell itself is able to absorb light more efficiently compared to the near infrared region. Other samples also showed efficiency increases of 5.1%.

Particle morphology can be correlated with response function measurements and efficiency enhancements to obtain a physics-based understanding of the optimization. Selected SEM images were analyzed according to histograms and wavelet analysis to obtain percent coverage and particle size distributions, respectively.

The role of plasma oscillations can be elucidated by correlating efficiency improvements with PEEM images of resonance hot-spot distributions. These “hot spots” are regions of near field enhancements and they can be correlated with PV measurements. It is desirable to have a maximum number of “hotspots” while we step up the light source in the range of 400-800 nm, so PEEM provides possibilities for the optimization of gold-black layers.

Electrodynamic simulations were performed on a system consisting of a silicon wafer substrate, gold particles, and polarized light. We saw field enhancement of an order of magnitude due to scattering and enhanced field bleeding out from the side of the slab, confirming that the field was being channeled inside the silicon substrate increasing the optical path length of the incident field. Simulations show great potential for further rapid optimization of the gold-black layers, once the dependence of film morphology on deposition parameters is understood.

Future work includes the expansion to aluminum- and silver-black thin films. Silver has high conductivity compared to aluminum, although both are more prone to oxidation than is gold. Impregnation of the porous films with polymer vapors [19] may improve adhesion and durability while protecting against oxidation. It also allows means to control the local dielectric environment of the metal particles to shift the resonances. Mixtures of different metal blacks with different plasma frequencies (e.g. Cu and Al) can be deposited with the goal of broadening the spectral response of the coating.

Using light trapping through resonant scattering by metal blacks, it is possible to construct optically thick but physically thin photovoltaics, which would be able to harvest the full solar spectrum. Thus the use of plasmonic nanoparticles allows completely new solar cell designs which could be highly efficient while consuming much less material.

ACKNOWLEDGMENTS

This work was supported by AFOSR STTR Phase I award FA9550-10-C-0069. We gratefully acknowledge the support of Dr. Gernot Pomrenke for this award. WPH, KNB, AJG, and SJP were supported by the Department of Energy, Office of Basic Energy Sciences, Division of Chemical Sciences, Geosciences, and Biosciences; Pacific Northwest National Laboratory (PNNL) is operated for the U.S. Department of Energy by Battelle. PEEM and the electrodynamic simulations were performed at EMSL, a national scientific user facility sponsored by the Department of Energy's Office of Biological and Environmental Research and located at PNNL. JC and KB were supported by the National Aeronautics and Space Administration under Grant No. NNX10AF20G issued through the Cassini Data Analysis Program.

REFERENCES

[1] Harry A. Atwater and Albert Polman, Nature Mater **9**, 205 (2010).
[2] K.R. Catchpole and A.Polman, Appl. Phys. Lett. **93**, 191113 (2008), Opt. Expr. **16**, 21793 (2008).
[3] L. Harris, R. T. McGinnies, and B. M. Siegel, "The Preparation and Optical Properties of Gold Blacks," J. Opt. Soc. Am. **38**, 582-589 (1948).
[4] L. Harris and J. K. Beasley, "The Infrared Properties of Gold Smoke Deposits," J. Opt. Soc. Am. **42**, 134-140 (1952).
[5] L. Harris and A. L. Loeb, "Conductance and Relaxation Time of Electrons in Gold Blacks from Transmission and Reflection Measurements in the Far Infrared," J. Opt. Soc. Am. **43**, 1114-1118 (1953).
[6] L. Harris, "The Transmittance and Reflectance of Gold Black Deposits in the 15- to 100-Micron Region," J. Opt. Soc. Am. **51**, 80-82 (1961).
[7] L. Harris and P. Fowler, "Absorptance of Gold in the Far Infrared," J. Opt. Soc. Am. **51**, 164-167 (1961).
[8] J.S.Bieteen, D.Pacific, N.S.Lewis, & H.A. Atwater, "Enhanced radiative emission rate and quantum efficiecy in coupled silicon nanocrystal-nanostructured gold emitters", Nano Lett. **5**, 1768 (2005).
[9] K.R. Catchpole, "Nanostructures in photovoltaics", Phil. Trans. R. Soc. A **364**, 3493-3503 (2006).
[10] S.Pillai & M.A. Green, "Plasmonics for photovoltaic applications", Solar energy Materials & Solar Cells **94** 1481-1486 (2010).
[11] C. Doland, P. O'Neill, and A. Ignatiev, "Particulate nature of solar absorbing films: Gold black," J. Vac. Sci. Tech. **14**, 259-262 (1977).
[12] P. O'Neill, C. Doland, and A. Ignatiev, "Structural composition and optical properties of solar blacks: gold black," Applied Optics **16**, 2822-2826 (1977).
[13] N. Nelms and J. Dowson, "Goldblack coating for thermal infrared detectors," Sensors and Actuators A. **120**, 403-407 (2005).
[14] A. H. Pfund, "The Optical Properties of Metallic and Crystalline Powders," J.O.S.A. **23**, 375-378 (1933).
[15] Justin W. Cleary, Robert E. Peale, Masahiro Ishigami, Christian W. Smith, Kevin Baillie, Josh E. Colwell, Oliver Edwards and Chris Fredricksen, J. Materials Science and Engineering 5, 171-176 (2011).
[16] c. Donald, P. O'Neill, and A. Ignatiev "Perticulate nature of solar absorbing films: Gold Black" J.Vac Sci. Technol., Vol 14 No.1 (1977).
[17] Yu A Akimov and W S Koh, "Resonant and nonresonant Plasmonic nanoparticles enhancement for thin-film silicon solar cells," Nanotechnology **21**, 235201 (2010).
[18] Wolf, S. and Tauber, R. N., [Silicon Processing for the VLSI Era, Vol. 1: Process Technology], Lattice Press, Sunset Beach, CA, chapter 18 (1986).
[19] Justin W. Cleary, Robert E. Peale, Masahiro Ishigami, Christian W. Smith, Kevin Baillie, Josh E. Colwell, Oliver Edwards, and Chris J. Fredricksen, "Effects of Polymer Infusion and Characteristic Length Scale on Gold-Black Long-Wave and Far-Infrared Absorbance," Journal of Materials Science and Engineering 5, 171-176 (2011).